

# ZnS–ZnO nanocomposites: synthesis, characterization and enhanced photocatalytic performance

Qun Ma<sup>1</sup> · Zhengshu Wang<sup>1</sup> · Hanxiang Jia<sup>1</sup> · Yongqian Wang<sup>1</sup>

Received: 26 February 2016 / Accepted: 31 May 2016 / Published online: 3 June 2016  
© Springer Science+Business Media New York 2016

**Abstract** ZnS–ZnO nanocomposites (NCs) were successfully synthesized via thermal treatment of as-synthesized ZnS nanostructured spheres (NSs). By applying multiple characterization technology, such as XRD, FESEM, EDS and UV–Vis, the obtained samples were fully characterized. After modification, the light-absorption performance of ZnS NSs to visible light was significantly enhanced. The band gap of ZnS–ZnO NCs was estimated to be 2.7 eV. The photocatalytic test indicated that ZnS–ZnO NCs exhibited enhanced photocatalytic activity in contrast to the pristine ZnS due to the effective charge separation. A photocatalytic mechanism was proposed to illustrate the photocatalytic reduction process. The formation mechanism of ZnS NSs and ZnS–ZnO NCs was also proposed in detail.

## 1 Introduction

Over the past decades, semiconductor materials have attracted worldwide attention to their potential applications in photodegradation of organic pollutants and hydrogen production with water splitting [1–6]. Metal sulfide semiconductors, such as ZnS, have attracted considerable attention in recent years due to their excellent properties in the photocatalytic fields [7–10].

As an important II–VI semiconductor with a wide band gap, ZnS is a well-known photocatalysts due to its stable and outstanding properties. However, the majority of

the synthesized ZnS photocatalysts still remains a relative low photodegradation efficiency because of its limitation of fairly wide band gap of ZnS (3.7 eV), which results in the absorption of UV-light in solar spectrum. However, as we all know, the solar spectrum only contains ~5 % of UV-light. Therefore, how to broaden the photo-response and enhance the photodecomposition efficiency of ZnS is a deserving research subject for scientists. Recently, to exploit well-defined nanocomposites is considered as a promising way. For example, ZnS–ZnO nanocomposites with different morphologies have been paid much attention due to their sizes, morphology-related properties and favourable photocatalytic properties [11–16]. However, currently, the facile synthesis of well-crystallized, cost-effective and novel ZnS–ZnO nanocomposites with enhanced photocatalytic activity still remains a challenge for scientific research.

In the work, we reported the synthesis of ZnS–ZnO nanocomposites (NCs) via a facile thermal treatment of ZnS nanostructured spheres (NSs). The thermal treatment is straightforward and low-cost to synthesize ZnS–ZnO nanocomposites. The formation mechanism of ZnS NSs and ZnS–ZnO NCs was illustrated in detail. Meanwhile, the photocatalytic activity of was investigated against methylene blue and the mechanism was discussed in detail.

## 2 Experimental section

### 2.1 Preparation of ZnS NSs

All the reagents in the present investigation were of analytical grade and used without further purification throughout the whole experimental process. Deionized water was used for preparation of all solution. In a typical

✉ Yongqian Wang  
cugwyq@126.com

<sup>1</sup> Faculty of Material Science and Chemistry, China University of Geosciences, Wuhan 430074, China

experimental process,  $\text{Zn}(\text{COOH})_2 \cdot 2\text{H}_2\text{O}$  [ $\text{Zn}(\text{AC})_2$ , 0.1 mol, 1.7560 g] was dissolved into 80 ml of deionized water under magnetic stirring. Subsequently,  $\text{NH}_2\text{CSNH}_2$  (thiourea, 0.1 mol, 0.6090 g) was added directly into mentioned-above solution containing  $\text{Zn}(\text{AC})_2$ . Then, the mixed solution was transferred into a 100 ml Teflon-lined stainless steel autoclave, heated and maintained at 140 °C for 8 h and cooled down to the room temperature. The samples were obtained by centrifugation, washed with deionized water and ethanol for some times. The final products were dried at 70 °C for 4 h. Besides, ZnS NSs were also synthesized by adjusting the starting ratio of Zn:S to 1:2, 1:4 and 1:6, respectively.

## 2.2 Synthesis of ZnS–ZnO NCs

Based on Fu's report [17], a certain amount of as-synthesized ZnS NSs were calcined in a muffle furnace at 500 °C for 2 h in air. The deep-green products were obtained for characterization with appropriate analytical techniques.

## 2.3 Characterization

The synthesized samples were characterized with multiple technologies. The general morphology of the synthesized samples was investigated with field emission scanning electron microscopy (FESEM, SU8010, HITACHI). The samples were pretreated with a thin amorphous gold on their surface before FESEM analysis. The element composition of the samples was measured with energy dispersive X-ray spectrometer (EDS) attached to the FESEM. The structure and crystal phase of the samples were characterized by powder X-ray diffraction (XRD, D8 Advanced XRD, BrukerAXS). UV–vis diffuse reflectance spectra were recorded with an UV–vis spectrophotometer (UV-3600, Shimadzu, Tokyo, Japan).

## 2.4 Photocatalytic tests

Photocatalytic performance of as-synthesized samples was evaluated through measuring the degradation efficiency of methylene blue with the presence of photocatalysts. Before photocatalytic test, all mixed solution with photocatalysts and methylene blue were placed in dark environment for 1 h to reach adsorption equilibrium, and then the residual concentration of methylene blue was measured. In a typical experiment, a 250 W high pressure mercury lamp was used. The lamp was placed 8 cm above the liquid surface. Subsequently, 0.1 g of photocatalysts was added into a 100 ml of  $1 \times 10^{-5}$  M methylene blue aqueous solution. The mixed solution was stirred constantly in the process of experiment. For a given duration (30 min), 3 ml solution was extracted to test the residual concentration of

methylene blue, which was evaluated by measuring the change of maximum absorbance in the UV–vis spectrometry (UV-3600, Shimadzu). The absorbent peak in about 664 nm was selected and the residual concentration was obtained though evaluating the intensity ratio between remained and original MB solution. The degradation rate was calculated as following equation:

$$\text{Degradation efficiency (\%)} = (C_0 - C) / C_0 \times 100\%$$

where  $C$  is the concentration of methylene blue at each irradiated time, and  $C_0$  is the initial concentration when adsorption–desorption equilibrium is achieved.

## 3 Results and discussion

### 3.1 Structural and morphological analysis

#### 3.1.1 ZnS NSs

To investigate the phase structures of ZnS NSs, X-ray diffraction was applied in the work. Figure 1 depicts the XRD pattern of ZnS NSs obtained at 1:1 of the starting ratio of Zn to S. The diffraction peaks of ZnS NSs at about  $2\theta = 27.9, 47.2,$  and  $56.3$  could be well in accord with the characteristic diffraction peaks of (111), (220), and (311) crystal faces of Blende ZnS with lattice constant of  $a = 5.3177 \text{ \AA}$  (JCPDS Card No. 79-0043). There were no other peaks of impurities, indicating the high purity of the ZnS NSs. In addition, the crystal size could be estimated according to Scherrer's Equation below:

$$D = (K\lambda) / (\beta \cos \theta)$$

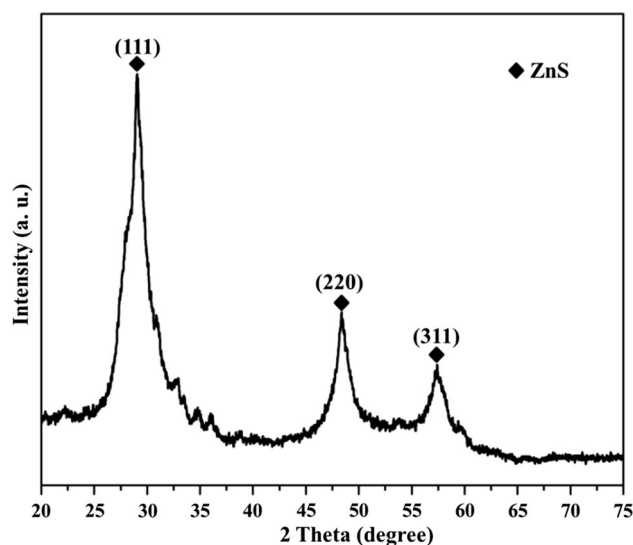


**Fig. 1** XRD pattern of pure ZnS NSs obtained at 1:1 of the starting ratio of Zn to S for 8 h at 140 °C

where  $D$  is the mean diameter of the crystallite,  $K$  is a constant related to the dimensionless shape (where  $k = 0.89$  in this case),  $\lambda$  is the wavelength of X-ray (where  $\text{Cu K}\alpha = 0.154056 \text{ nm}$ ),  $\beta$  is the full width half maximum of the intensity (FWHM), and  $\theta$  is the corresponding Bragg angle. The obtained average size was 7.2 nm.

As depicted in Fig. 2, it can be observed that the ZnS products synthesized with different concentration of sulfur sources were uniform and well-dispersed. One can see that the ZnS NSs turn to be aggregative with the increasing of concentration of sulfur sources, which decreased the dispersibility of NSs. The average diameter was estimated to be  $\sim 2.2 \mu\text{m}$ . Moreover, it is noticed that the sizes of ZnS NSs were slightly diverse, which can be attributed to the fast crystallization rate of ZnS crystals due to abundant  $\text{S}^{2-}$  in initial hydrothermal reaction. The variety of morphology and size indicated concentration of sulfur sources has an effect on the formation process of ZnS NSs.

### 3.1.2 ZnS–ZnO NCs

As depicted in Fig. 3, the ZnS–ZnO NCs exhibit significantly different features in the XRD patterns, in contrast to pristine ZnS NSs synthesized with 1:1 of Zn source to S source. One can notice that the XRD pattern of ZnS–ZnO NCs contains some obvious diffraction peaks, which belong to hexagonal ZnO structure (JCPDS Card No. 36-1451). The presence of ZnO diffraction peaks indicates the successful decoration of ZnO shells onto ZnS cores. Besides, it is worth noting that the diffraction peak of (111)

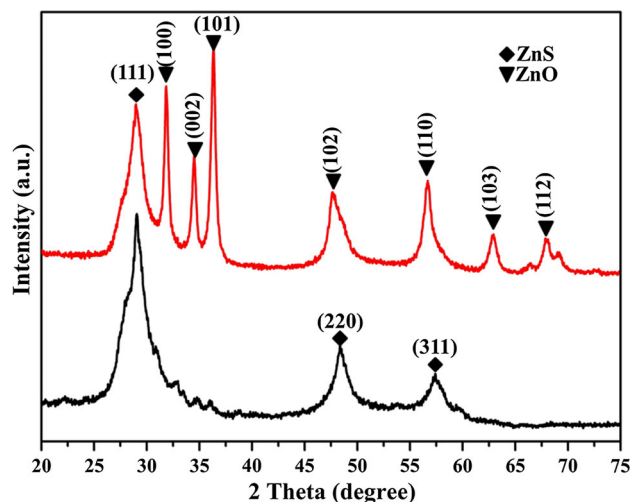
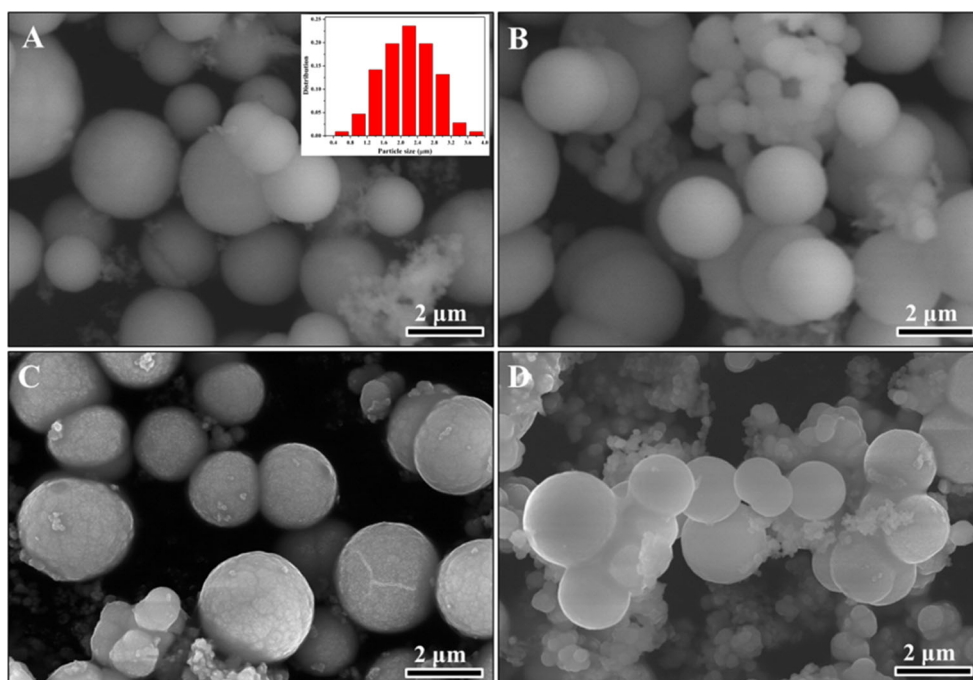


**Fig. 3** XRD patterns of ZnS NSs and ZnS–ZnO NCs

plane of ZnS NSs still remains in the pattern, which can be attributed to the partial oxidation of ZnS cores.

Figure 4 shows FESEM images of ZnS NSs synthesized with 1:1 of Zn source to S source and ZnS–ZnO NCs. Compared with pristine ZnS NSs, ZnS–ZnO NCs also present spherical structure. However, its surface structure is changed slightly. Meanwhile, ZnS–ZnO NCs contain of some nanosheets, which was not observed in the ZnS NSs. The variety of surface structure and the appearance of nanosheets may be attributed surface oxidation of ZnS NSs after experienced thermal treatment (as depicted in Fig. 4b). Further investigations of compositions of ZnS–

**Fig. 2** FESEM images of ZnS NSs synthesized at different initial molar ratio of Zn to S at  $140^\circ\text{C}$  for 8 h. **a** 1:1, **b** 1:2, **c** 1:4, and **d** 1:6. The inset in **a** is the size distribution



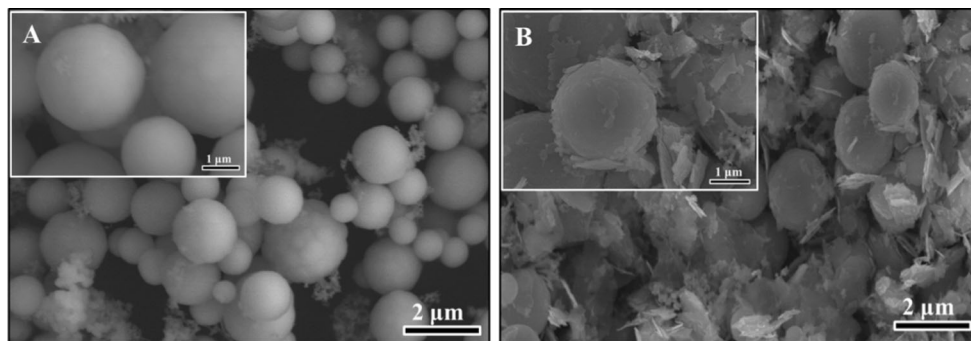
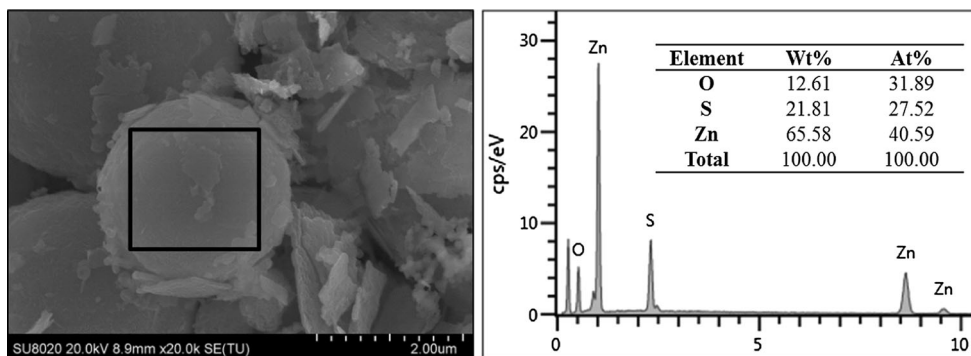


**Fig. 4** FESEM images of obtained samples, (a) ZnS NSs, (b) ZnS–ZnO NCs

**Fig. 5** EDS spectrum of ZnS–ZnO NCs

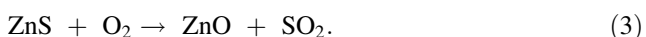
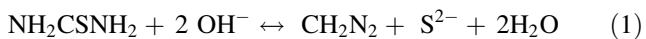


ZnO NCs have been performed through EDS measurement, as discussed below.

Figure 5 depicts the EDS spectrum of ZnS–ZnO NCs. The EDS spectrum agrees with the XRD results. The presence of Zn, S and O element exhibits that ZnS–ZnO NCs were synthesized successfully via thermal treatment of ZnS NSs. It was founded that there were no other elements of impurities, which indicated the high quality of products was synthesized. On the basis of atom ratio of S, the atom ratio of Zn in ZnS can be obtained to be 27.52 %. Subsequently, the atom ratio of Zn in ZnO was calculated to be 13.07 %. Finally, the molar ratio of ZnS/ZnO was calculated to be 2:1. And the mass ratio of ZnS/ZnO was 3:1.

### 3.2 Growth mechanism

The formation process of ZnS NSs and ZnS–ZnO NCs are illustrated in Fig. 6. The entire reaction were presented in the following equations [18]:



When the reaction temperature comes up to certain value, the thiourea begins to release  $\text{S}^{2-}$  ions slowly and

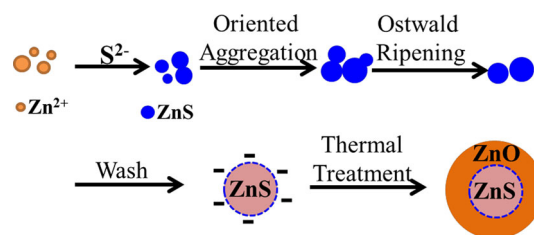


**Fig. 6** Schematic illustration of formation of ZnS NSs and ZnS–ZnO NCs

homogeneously [reaction (1)]. Then  $\text{Zn}^{2+}$  ions in the aqueous solution react with  $\text{S}^{2-}$  ions forming ZnS nanocrystals [reaction (2)]. In the present work, because we did not use any templates or capping agent, the formation of ZnS NSs may be attributed to oriented aggregation of nanoparticles and Ostwald ripening process. When ZnS NSs were experiencing the thermal treatment in air at 500 °C, the external ZnS crystals would react with oxygen in air to form ZnO crystals [reaction (3)]. Hence, ZnS–ZnO NCs were obtained after thermal treatment of ZnS NSs. Interestingly, as shown in Fig. 4b, a large number of nano sheets were synthesized, which may result from the separation between external primary ZnO crystals and internal secondary ZnO crystals, driven by the stress inside crystals under high temperature.



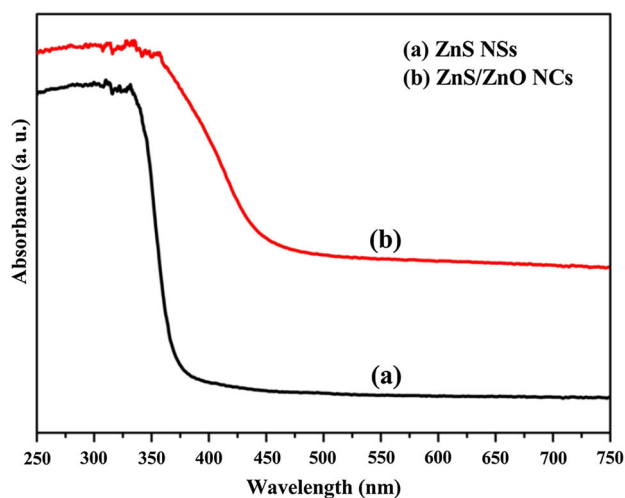


**Fig. 7** UV-Vis spectra and  $(\alpha h\nu)^2$  versus  $h\nu$  plot of pristine ZnS NSs and ZnS-ZnO NCs

### 3.3 Optical properties

The UV-Vis spectra and  $(\alpha h\nu)^2$  versus  $h\nu$  plot of pristine ZnS NSs synthesized with 1:1 of Zn source to S source and ZnS-ZnO NCs have been recorded and measured (Fig. 7). As shown in Fig. 7, after experienced a thermal treatment, the absorption edge of ZnS has a significant shift to long wavelength (we called red-shift of absorption edge). Meanwhile, one can see that the light absorption of ZnS in the visible range is highly enhanced, which will facilities the utilize efficiency of solar light. In contrast to pristine ZnS NSs, the enhancement of absorption of ZnS-ZnO NCs in the visible range can be attributed to the abundant presence of defects. It is known that photocatalytic activity of materials depend on the light absorption. Hence, it is believed that the ZnS-ZnO NCs may possess well photocatalytic performance. It has been reported that partial conversion from ZnS to ZnS-ZnO nanocrystals can lead to

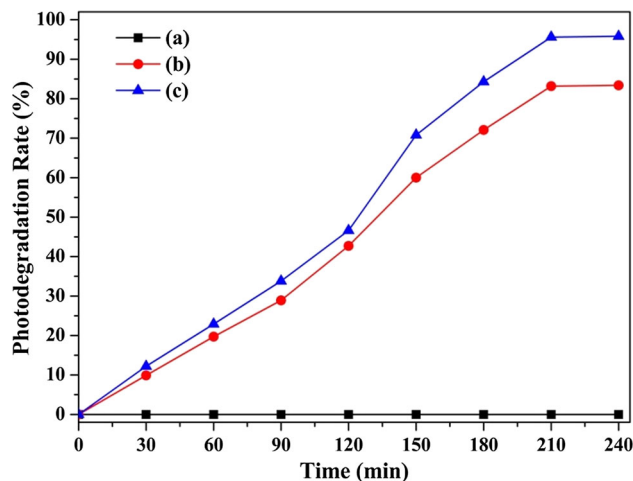


**Fig. 8** The photodegradation rate of methylene blue in the presence of photocatalysts, (a) without photocatalysis, (b) pure ZnS NSs, (c) ZnS-ZnO NCs

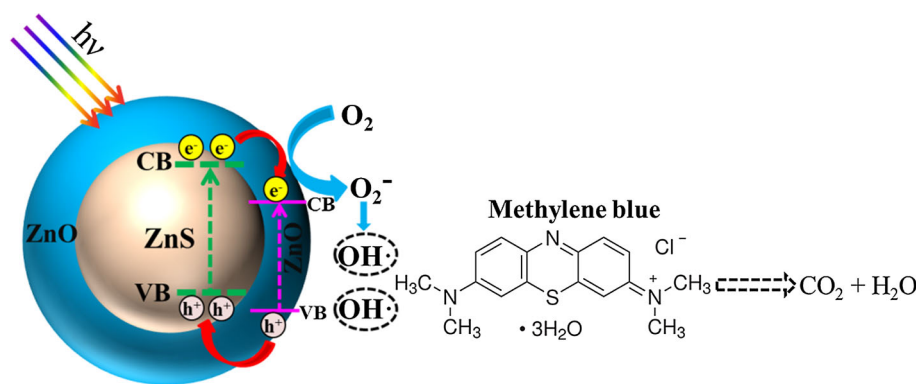
a change of band-gap and absorption ability [19]. According to the  $(\alpha h\nu)^2$  versus  $h\nu$  plot, we can calculated the band gap of pristine ZnS NSs and ZnS-ZnO NCs to be 3.4 and 2.7 eV, respectively. On the basis of the results, one can believe that after experienced thermal treatment, the photocatalytic activity of ZnS was enhanced due to the decoration of ZnO.

### 3.4 Photocatalytic activity

The photocatalytic degradation of methylene blue is chosen a model reaction to evaluate the photocatalytic performance of ZnS NSs and ZnS-ZnO NCs. The test without the presence of photocatalysts was as blank group. The degradation results were presented in Fig. 8. The methylene blue was not decomposed with the absence of photocatalysts. With the presence of ZnS and ZnS-ZnO NCs, the degradation of methylene blue was obvious under the illumination of light. After 60 min of reaction, the photodegradation efficiencies of methylene blue are about 20 and 25 % for the ZnS NSs and ZnS-ZnO NCs, respectively. For the ZnS NSs, only about 80 % of methylene blue was photocatalytically degraded within 4 h. And for the nanocomposites, the photocatalytic efficiency can reach up to 95 %. Obviously, the degradation ability of ZnS-ZnO NCs was better than pristine ZnS NSs. The reason was discussed in detail as below.

Figure 9 was applied to illustrate the photocatalytic reduction process. Under the light illumination, ZnO and ZnS are excited and electron-hole pairs are generated. According to the report, the excited electrons in the CB of ZnS diffuse into the CB of ZnO to achieve a balance in Fermi energy level equilibration because the conduction band potential of the ZnS is more negative than that of the

**Fig. 9** Schematic illustration of the photocatalytic mechanism of as-synthesized ZnS–ZnO NCs



ZnO [20], during which more active charges would be produced as a result of better charge separation [21]. Meanwhile, the electrons in the CB of ZnO immigrate to the surface of photocatalysts. Subsequently, these electrons would react with dissolved oxygen molecules, forming super-oxide radical anion ( $O_2^{\cdot-}$ ). And then  $O_2^{\cdot-}$  would further turn into highly reactive hydroxide radicals ( $OH\cdot$ ). Due to the high oxidation activity, the formed  $OH\cdot$  would decompose the methylene blue into  $CO_2$  and  $H_2O$ . In this manner, the photocatalytic performance of ZnS NSs was significantly enhanced by the surface-modification with ZnO.

#### 4 Conclusions

In summary, ZnS–ZnO nanocomposites (NCs) were successfully synthesized via thermal treatment of ZnS nanostructured spheres (NSs). Compared with others method, the thermal treatment is straightforward and low-cost to synthesize different nanocomposites. On the basis of characterization, the formation of ZnS NSs may be attributed to oriented aggregation of nanoparticles and Ostwald ripening process. After decoration of ZnO, the light absorption of ZnS NSs was enhanced obviously range from UV light to visible light. The band gap of ZnS–ZnO NCs was estimated to be 2.7 eV, obviously decreasing compared with 3.4 eV of pristine ZnS NSs. The photocatalytic test indicated that the synthesized ZnS–ZnO NCs exhibited enhanced photocatalytic performance in contrast to the pristine ZnS because of effective charge separation. It is believed that the facile method will make more researchers investigate and optimize ZnS–ZnO system and the photocatalysis will possess wide application in environmental fields.

**Acknowledgments** This work was supported by the Fundamental Research Funds for the Central Universities, China University of Geosciences (Wuhan, CUG120118). The financial support was gratefully appreciated.

#### References

- H.L. Wang, L. Zhang, Z. Chen, J.Q. Hu, S.J. Li, Z.H. Wang, J.S. Liu, X.C. Wang, Semiconductor heterojunction photocatalysts: design, construction, and photocatalytic performances. *Chem. Soc. Rev.* **43**, 5234–5244 (2014)
- Q.J. Xiang, J.G. Yu, M. Jaroniec, Enhanced photocatalytic  $H_2$ -production activity of graphene-modified titania nanosheets. *Nanoscale* **3**, 670–678 (2011)
- K. Shimuraa, H. Yoshida, Heterogeneous photocatalytic hydrogen production from water and biomass derivatives. *Energy Environ. Sci.* **4**, 2467–2481 (2011)
- M.H. Luo, W.F. Yao, C.P. Huang, Q. Wu, Q.J. Xu, Shape effects of Pt nanoparticles on hydrogen production via Pt/CdS photocatalysts under visible light. *J. Mater. Chem.* **3**, 13884–13891 (2015)
- K. Zhang, L.J. Guo, Metal sulphide semiconductors for photocatalytic hydrogen production. *Catal. Sci. Technol.* **3**, 1672–1690 (2013)
- S. Protti, A. Albin, N. Serpone, Photocatalytic generation of solar fuels from the reduction of  $H_2O$  and  $CO_2$ : a look at the patent literature. *Phys. Chem. Chem. Phys.* **16**, 19790–19827 (2014)
- S.L. Xiong, B.J. Xi, C.M. Wang, D.C. Xu, X.M. Feng, Z.C. Zhu, Y.T. Qian, Tunable synthesis of various wurtzite ZnS architectural structures and their photocatalytic properties. *Adv. Funct. Mater.* **17**, 2728–2738 (2007)
- F.F. Shi, L.L. Chen, C.S. Xing, D.L. Jiang, D. Li, M. Chen, ZnS microsphere/g-C $_3$ N $_4$  nanocomposite photocatalyst with greatly enhanced visible light performance for hydrogen evolution: synthesis and synergistic mechanism study. *RSC Adv.* **4**, 62223–62229 (2014)
- R. Michael, J. Theerthagiri, J. Madhavan, M.J. Umapathy, P.T. Manoharan,  $Cu_2S$ -incorporated ZnS nanocomposites for photocatalytic hydrogen evolution. *RSC Adv.* **5**, 30175–30186 (2015)
- X.T. Wang, L. Rong, K. Wang, Synthesis of ZnO@ZnS– $Bi_2S_3$  core-shell nanorod grown on reduced graphene oxide sheets and its enhanced photocatalytic performance. *J. Mater. Chem. A* **2**, 8304–8313 (2014)
- H. Zhao, Y.M. Dong, P.P. Jiang, X.M. Wu, R.X. Wu, Y.M. Chen, Facile preparation of a ZnS/ZnO nanocomposite for robust sunlight photocatalytic  $H_2$  evolution from water. *RSC Adv.* **5**, 6494–6500 (2015)
- Z. Wang, W.C. Shao, C. Xue, Nanoparticle heterojunctions in ZnS–ZnO hybrid nanowires for visible-light-driven photocatalytic hydrogen generation. *CrystEngComm* **15**, 5688–5693 (2013)

13. X.X. Gao, J. Wang, J.L. Yu, H.B. Xu, Novel ZnO–ZnS nanowire arrays with heterostructures and enhanced photocatalytic properties. *CrystEngComm* 2015, *Advance Article*
14. S.S. Lo, Y.T. Hung, D.J. Jan, Stress induction, UV emission variation and efficiency variation in dye-sensitized solar cells of hollow ZnS/ZnO/ZnS nanostructures. *J. Mater. Chem. A* **1**, 10274–10280 (2013)
15. Z.Q. Wang, Z. Liu, J.F. Gong, S. Wang, S.G. Yang, Structure and optical properties of individual hierarchical ZnS nanobelt/ZnO nanorod heterostructures. *CrystEngComm* **13**, 6774–6779 (2011)
16. J. Luo, S.Q. Zhao, P.P. Wu, K. Zhang, C. Peng, S.W. Zheng, Synthesis and characterization of new Cd-doped ZnO/ZnS core-shell quantum dots with tunable and highly visible photoluminescence. *J. Mater. Chem. C* **3**, 3391–3398 (2015)
17. X.H. Fu, X.F. Yang, Z.R. Qiu, F.H. Zhao, J.L. Zhuang, A.H. He, L.Q. Chen, C.L. Wu, X.J. Duan, C.L. Liang, M.M. Wu, Outward conversion of core-shell nanostructured Zn Smicrospheres to mesoporous ZnO ones. *CrystEngComm* **15**, 3334–3340 (2013)
18. Y. Liu, J.C. Hu, C. Ngo et al., Gram-scale wet chemical synthesis of wurtzite-8H nanoporous ZnS spheres with high photocatalytic activity. *Appl. Catal. B* **106**, 212–219 (2011)
19. J. Schrier, D.O. Demchenko, L. Wang, Optical properties of ZnO/ZnS and ZnO/ZnTe heterostructures for photovoltaic applications. *Nano Lett.* **7**, 2377–2382 (2007)
20. E. Hong, J.H. Kim, Oxide content optimized ZnS–ZnO heterostructures via facile thermal treatment process for enhanced photocatalytic hydrogen production. *J. Hydrogen Energy* **39**, 9985–9993 (2014)
21. T.K. Jana, A. Pal, K. Chatterjee, Self-assembled flower like CdS–ZnO nanocomposite and its photocatalytic activity. *J. Alloy. Compd.* **583**, 510–515 (2014)